

# UC Irvine

## UC Irvine Previously Published Works

### Title

A large animal model of RDH5-associated retinopathy recapitulates important features of the human phenotype.

### Permalink

<https://escholarship.org/uc/item/2623r6z7>

### Journal

Human Molecular Genetics, 31(8)

### Authors

Ocelli, Laurence  
Daruwalla, Anahita  
De Silva, Samantha  
et al.

### Publication Date




2022-04-22

### DOI

10.1093/hmg/ddab316

Peer reviewed

# A large animal model of *RDH5*-associated retinopathy recapitulates important features of the human phenotype

Laurence M. Occelli<sup>1,†</sup>, Anahita Daruwalla <sup>2,3,†</sup>, Samantha R. De Silva<sup>4,5</sup>, Paige A. Winkler<sup>1</sup>, Kelian Sun<sup>1</sup>, Nathaniel Pasmanter<sup>1</sup>, Andrea Minella<sup>1</sup>, Janice Querubin<sup>1</sup>, Leslie A. Lyons<sup>6</sup>, 99 Lives Consortium<sup>‡</sup>, Anthony G. Robson<sup>4,5</sup>, Elise Heon<sup>7,8,9</sup>, Michel Michaelides<sup>4,5</sup>, Andrew R. Webster<sup>4,5</sup>, Krzysztof Palczewski <sup>2,10,11</sup>, Ajoy Vincent<sup>7,8,9</sup>, Omar A. Mahroo<sup>4,5,12,13</sup>, Philip D. Kiser<sup>2,10,14</sup> and Simon M. Petersen-Jones <sup>1,\*</sup>

<sup>1</sup>Department of Small Animal Clinical Sciences, Michigan State University, East Lansing, MI 48824, USA

<sup>2</sup>Department of Physiology & Biophysics, University of California, Irvine School of Medicine, Irvine, CA 92697, USA

<sup>3</sup>Department of Pharmacology, Case Western Reserve University, Cleveland, OH 44106, USA

<sup>4</sup>Moorfields Eye Hospital NHS Foundation Trust, London, UK

<sup>5</sup>UCL Institute of Ophthalmology, University College, London, UK

<sup>6</sup>Department of Veterinary Medicine and Surgery, College of Veterinary Medicine, University of Missouri, Columbia, MO 65211, USA

<sup>7</sup>Genetics and Genome Biology, The Hospital for Sick Children, Toronto, Canada

<sup>8</sup>Institute of Medical Science, The University of Toronto, Toronto, Canada

<sup>9</sup>Department of Ophthalmology and Vision Sciences, The Hospital for Sick Children, Toronto, Canada

<sup>10</sup>Department of Ophthalmology, Gavin Herbert Eye Institute, Center for Translational Vision Research, University of California, Irvine, CA 92617, USA

<sup>11</sup>The Department of Chemistry, Department of Molecular Biology and Biochemistry, University of California, Irvine, CA 92697, USA

<sup>12</sup>Section of Ophthalmology, King's College London, St Thomas' Hospital Campus, London, UK

<sup>13</sup>Physiology, Development and Neuroscience, University of Cambridge, Cambridge, UK

<sup>14</sup>Research Service, The Veterans Affairs Long Beach Health Care System, Long Beach, CA 90822, USA

\*To whom correspondence should be addressed at: 736 Wilson Road, D208, Veterinary Medical Center, Michigan State University, East Lansing, MI 48824, USA.

Tel: +1 5173533278; Email: peter315@msu.edu

<sup>†</sup>These authors contributed equally to this work.

<sup>‡</sup>For consortium members see [Supplementary Material](#).

## Abstract

Pathogenic variants in retinol dehydrogenase 5 (*RDH5*) attenuate supply of 11-*cis*-retinal to photoreceptors leading to a range of clinical phenotypes including night blindness because of markedly slowed rod dark adaptation and in some patients, macular atrophy. Current animal models (such as *Rdh5*<sup>-/-</sup> mice) fail to recapitulate the functional or degenerative phenotype. Addressing this need for a relevant animal model we present a new domestic cat model with a loss-of-function missense mutation in *RDH5* (c.542G > T; p.Gly181Val). As with patients, affected cats have a marked delay in recovery of dark adaptation. In addition, the cats develop a degeneration of the *area centralis* (equivalent to the human macula). This recapitulates the development of macular atrophy that is reported in a subset of patients with *RDH5* mutations and is shown in this paper in seven patients with biallelic *RDH5* mutations. There is notable variability in the age at onset of the *area centralis* changes in the cat, with most developing changes as juveniles but some not showing changes over the first few years of age. There is similar variability in development of macular atrophy in patients and while age is a risk factor, it is hypothesized that genetic modifying loci influence disease severity, and we suspect the same is true in the cat model. This novel cat model provides opportunities to improve molecular understanding of macular atrophy and test therapeutic interventions for *RDH5*-associated retinopathies.

## Introduction

The classical visual (retinoid) cycle involves shuttling retinoids from the photoreceptor to the retinal pigment epithelium (RPE) within which a series of enzymatic steps occur resulting in the regeneration of 11-*cis*-retinal for transport back to the photoreceptor allowing regeneration of active visual pigment. For a recent review of the visual cycle see Daruwalla *et al.* (1). The final enzymatic step in the visual cycle within the RPE is the oxidation of 11-*cis*-retinol to 11-*cis*-retinal. The main enzyme that

catalyzes this reaction is 11-*cis*-retinol dehydrogenase (gene retinol dehydrogenase 5, *RDH5*: OMIM No. 601617), which belongs to the family of short-chain dehydrogenase/reductases (SDRs) (2). *RDH5* is membrane bound and in common with other SDRs likely exists as a dimer (3). It is essential for the normal dynamics of rod and cone visual pigment regeneration (4).

Abnormal visual cycle kinetics leads to a delay in rod and cone functional regeneration and a congenital night blindness (4–6). In addition, a range of clinical

phenotypes are associated with *RDH5* mutations, the most common of which is fundus albipunctatus (FA) (OMIM No. 136880), which is named for the bilateral appearance of whitish-yellow dots across the fundus with the exception of the fovea. On optical coherence tomography (OCT), the white dots appear as lesions that extend from the RPE into the outer segment layer, although their precise constituents are not known (7–11). The number of dots is reported to change with disease progression (12) and is not a feature in all patients with *RDH5*-associated retinopathy (8). Fundus autofluorescence imaging shows reduced autofluorescence or a grainy appearance suggesting reduced A2E (N-retinylidene-N-retinylethanolamine) and other retinoid condensation products because of the impairment of the visual cycle (9,13,14). Cone dysfunction is reported in many patients and can progress to a cone dystrophy (8,14–20). Some patients develop more severe retinal abnormalities involving the macula being variably described as bull's eye maculopathy, macular atrophy, or macular degeneration and cause severe vision loss and, in some instances, legal blindness. Although macular disease has been reported in patients as young as 9 years of age (21), the condition is more common in older patients (9,12,18,22–24).

Animal models of *RDH5*-associated retinopathy that recapitulate human disease would support the understanding of the disease mechanisms and the development and testing of therapies. An *Rdh5*<sup>-/-</sup> mouse has been generated (10), but unlike human subjects the mice had normal rod function on electrophysiological testing and only exhibited delayed dark adaptation after prolonged bleaching (10,25). One study found no gross or ultrastructural indications of photoreceptor loss at 2 months of age (26). Retinoid analysis showed that *Rdh5*<sup>-/-</sup> mice accumulate *cis*-retinoids, in particular 13-*cis* isomers, in the RPE (27). The relatively mild phenotype in the *Rdh5*<sup>-/-</sup> mouse is thought to indicate that other retinol dehydrogenases play a significant role in regeneration of 11-*cis*-retinal in this species (26,28).

In this study, we introduce a new cat model that recapitulates the human functional phenotype more consistently than prior mouse models. Furthermore, the affected cats develop the equivalent of macular atrophy, with variation in the age at onset. We also report the development of macular atrophy in seven patients with biallelic *RDH5* mutations.

## Results

### An *RDH5* missense mutation in cats with *area centralis* atrophy and slow rod recovery

The proband cat was obtained at 8 months of age from a commercial supplier of laboratory cats for an unrelated study. When first examined at just under 1 year of age, it was noted on indirect ophthalmoscopy and color fundus photography to have bilaterally symmetric abnormal hyporeflective lesions involving the *area*

*centralis* and visual streak (Fig. 1A). These retinal regions have higher photoreceptor packing density for higher acuity vision making the *area centralis* analogous to the human macula. With progression, retinal thinning developed at the *area centralis* and the area of retinal thinning enlarged with age. Spectral domain-optical coherence tomography (SD-OCT) showed retinal thinning with loss of the photoreceptor layers involving the *area centralis* (Fig. 1B–D). The hyporeflective lesions represent retinal regions with abnormally long and distorted photoreceptor outer segments (Fig. 1D middle image). With degeneration in the *area centralis*, the outer nuclear layer thins to a single layer of photoreceptor nuclei (Fig. 1D right image) compared with the normal 10–11 rows (Fig. 1D left image). An initial breeding study suggested that the *area centralis*/visual streak lesion segregated in an autosomal recessive fashion (see Supplementary Material, Fig. S1 for a partial pedigree of the colony). A trio of cats (two clinically affected and one obligate carrier) from the colony (see Supplementary Material, Fig. S1) were submitted for whole-genome sequencing (WGS) under the 99 lives consortium feline genome sequencing initiative. Three genes with known retinal expression were identified with missense variants that were private to the trio of cats and homozygous in the two affected cats and heterozygous in the obligate carrier (Supplementary Material, Table S1). The variants were genotyped in the larger pedigree and only the Gly181Val missense variant in *RDH5* was homozygous in all of the cats with the *area centralis* degeneration (Supplementary Material, Table S2).

Glycine residue at position 181 is highly conserved in mammalian *RDH5* orthologs (Fig. 1E). To evaluate the role of Gly181 in the structure and function of this enzyme, a homology model of the tertiary structure of *Felis catus* *RDH5* (FcRDH5) was created on the basis of the homodimer of 17 $\beta$ -hydroxysteroid dehydrogenase 1, which has 29.8% sequence identity with FcRDH5 (29). The enzyme was modeled as a dimer with Gly181 located at the dimer interface and in close proximity to catalytic site residues, particularly Lys179 (Fig. 1F). The Gly181 C $\alpha$  is buried at the dimer interface in van der Waals contact with Val177 and Gly181 of the opposing monomer. Substitution of G181 with a Val residue containing a much larger isopropyl side chain introduces severe steric clashes that cannot be resolved by simple rotamer switching. Hence, it is likely that mutation to Val residue at position 181 disrupts dimer formation and/or structure. Alternatively, if the dimer still forms, the structural distortions incurred to accommodate the bulkier side chain are likely to displace the nearby Lys179 residue resulting in loss of catalytic activity. Western blotting of RPE and retinal immunohistochemistry showed cats homozygous for Gly181Val *RDH5* mutation lacked detectable protein (Fig. 2A and B). Furthermore, the heterozygous cat showed a lower *RDH5* expression than wild type (WT) (Fig. 2A). Given the lack of detectable *RDH5* in the RPE of homozygous mutant cats, these

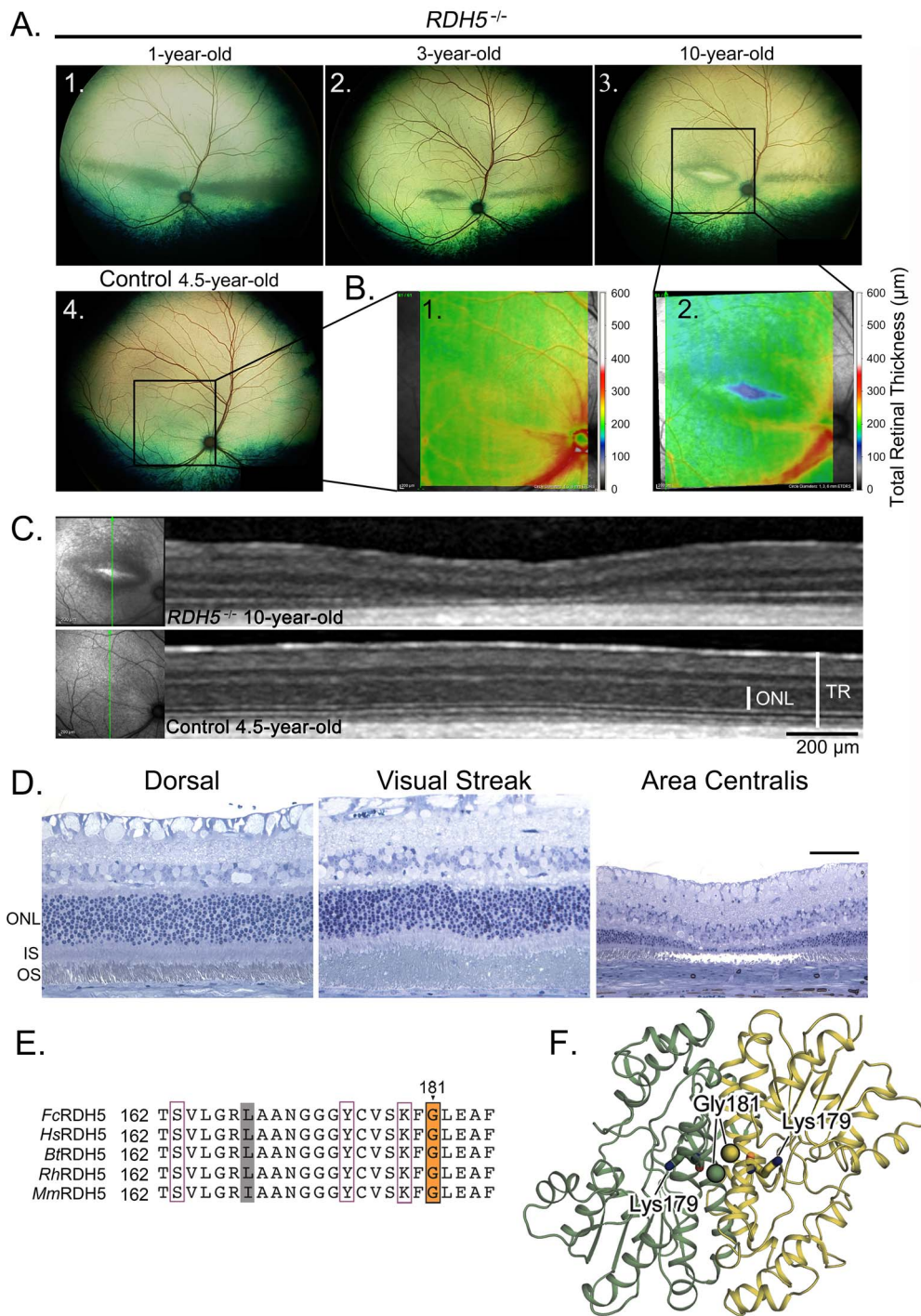


**Figure 1.** *RDH5* mutant cat model. **(A)** Color fundus images of the proband at first diagnosis at 1 year of age (A1) and at 3 (A2) and 10 (A3) years of age compared with a control cat at 4.5 years of age (A4). The affected cat initially has a band of hyporeflectivity encompassing the *area centralis* and visual streak. At 3 years of age, hyperreflectivity in the *area centralis* region was present, which is a clinical indicator of retinal thinning. By 10 years of age, the area of retinal thinning is enlarged to involve the entire *area centralis*. **(B)** Heat maps of the control cat in A4 (B1) and the 10-year-old affected cat in A3 (B2) showing retinal thickness in the *area centralis* region. The area imaged is shown with a black square superimposed on the color images. Note the severe retinal thinning in the *area centralis* of the affected cat. **(C)** SD-OCT images vertically through the *area centralis* of the affected cat at 10 years of age (upper) and the control cat (lower). The green lines on the infrared confocal scanning laser ophthalmoscopy (cSLO) images to the left show the plane of the cross-sectional images. Note the complete loss of the outer retinal layers in the affected cat in the *area centralis* compared with the retina of normal thickness of the control cat. TR, total retina; ONL, outer nuclear layer. **(D)** Semi-thin plastic sections from a 1.5-year-old affected cat. The unaffected dorsal retina shows normal photoreceptor outer segment arrangement. The visual streak shows lengthening and distortion of the outer segments corresponding to the appearance of regional fundus hyporeflectivity. The *area centralis* shows outer retinal degeneration with only one row of photoreceptor nuclei remaining. The size bar is 50 μm for the left two images and 100 μm for the *area centralis*. IS, inner segment; OS, outer segment. **(E)** Sequence alignment of *RDH5* orthologs. Protein sequences of *H. sapiens* *RDH5* (*HsRDH5*), *FcRDH5*, *Bos taurus* (*BtRDH5*), *Macaca mulatta* (*RhRDH5*) and *Mus musculus* (*MmRDH5*) aligned in ClustalW2 (49) and displayed with ESPript (50). The catalytic triad residues S163, Y175 and K179 are boxed in lilac. The site of mutation, Gly181 for *FcRDH5* is highlighted in an orange box. **(F)** Homology model of dimeric *FcRDH5* created using SwissModel (48). The two monomers are indicated as a green and yellow cartoon. Gly181 is shown as a sphere at the dimer interface. Lys179 of the catalytic triad is indicated as a stick to depict its close positioning to Gly181.

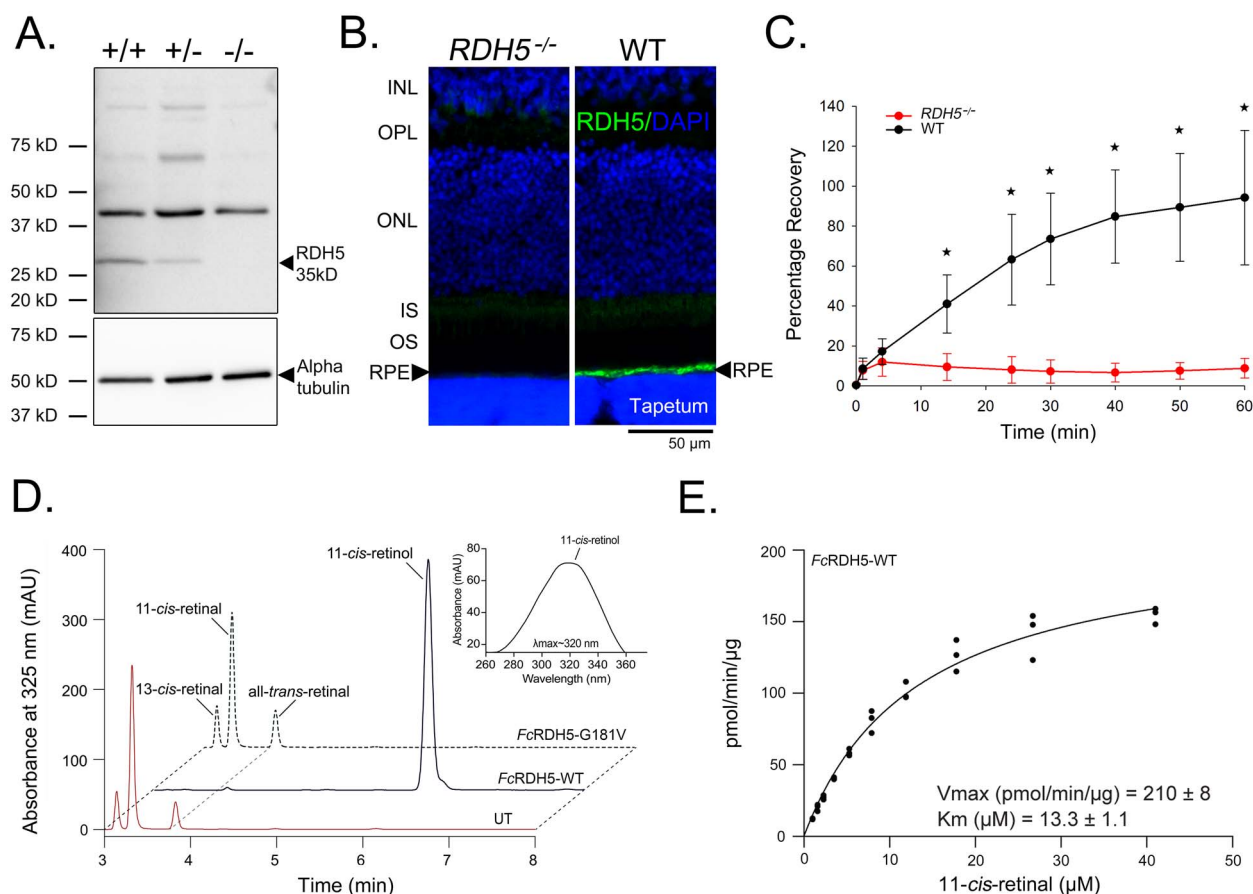


**Figure 2.** Effect of RDH5 Gly181Val mutation in the cat. **(A)** Western blot of RPE samples from  $RDH5^{+/+}$ ,  $RDH5^{+/-}$  and  $RDH5^{-/-}$  cats. The band corresponding to RDH5 is indicated by the arrowhead. Note the lack of RDH5 in the homozygous mutant cat and the reduced presence in the heterozygote. **(B)** IHC for RDH5 in a mutant and WT cat retinal section. Green is RDH5 and blue DAPI nuclear stain. INL, inner nuclear layer; OPL, outer plexiform layer; ONL, outer nuclear layer. **(C)** Plot of recovery of dark-adapted ERG b-wave (to a 0.01 cd-s/m<sup>2</sup> rod stimulating flash) following light exposure (30 cd/m<sup>2</sup> for 10 min) in WT and mutant cats. This shows percentage recovery to the pre-light exposure amplitude, which was recorded following overnight dark adaptation (mean  $\pm$  SD,  $n = 3$  WT and  $n = 4$   $RDH5^{-/-}$ ). This clearly shows the very delayed recovery of dark adaptation even following a moderate light exposure. \* $P < 0.05$  (t-test). **(D)** FcRDH5. Normal phase HPLC elution profile from activity assay of FcRDH5. Elution profile of retinoids from WT enzyme (FcRDH5-WT, solid trace) shows near complete conversion of 11-cis-retinol to 11-cis-retinol, whereas that obtained from the mutant (FcRDH5-Gly181Val, dashed trace) lacks 11-cis-retinol, indicating loss of its dehydrogenase function. Chromatography was performed using an isocratic flow of 80% hexane and 20% ethyl acetate over a period of 10 min. UT—untransfected control. **(E)** Michaelis-Menten steady-state kinetics for FcRDH5-WT using a range of 11-cis-retinal concentrations. The graph is plotted as substrate concentration [11-cis-retinal] ( $\mu$ M) versus initial reaction rate (pmol/min/ $\mu$ g). Computed kinetic parameters  $V_{max}$  (maximum reaction rate) and  $K_m$  (Michaelis-Menten constant) are denoted alongside the graph.

presumed structural distortions likely trigger rapid protein degradation.

Electroretinographic (ERG) studies showed that all  $RDH5^{-/-}$  cats tested ( $n = 10$ ) had a marked delay in restoration of rod function following exposure to a standard rod suppressing white light (30 cd/m<sup>2</sup> light for 10 min as used in the ISCEV full-field ERG protocol) (Fig. 2C). A small b-wave returned in the first 4 min of dark adaptation (similar to controls) but after that there was no further recovery over the subsequent 1 h. In contrast, WT cats (Fig. 2C) and  $RDH5^{+/-}$  cats (data not shown) showed recovery of the dark-adapted ERG within 1 h. The dark-adapted luminance:response series showed that following dark adaptation overnight the threshold and amplitude of responses of the  $RDH5^{-/-}$  cats were comparable to WT controls. The 1 h of dark-adaptation used in our standard cat scotopic ERG

protocol was insufficient for complete dark-adaptation in the  $RDH5^{-/-}$  cats.

### Activity of *F. catus* RDH5 mutant Gly181Val is abolished in vitro

To test whether the Gly181Val mutation impacts RDH5 expression and catalytic function *in vitro*, recombinant WT and Gly181Val FcRDH5 with C-terminal 1D4 tags were expressed in Sf9 insect cells and the membrane-bound proteins were isolated for activity assays (30). Immunoblotting with an anti-ID4 antibody showed comparable expression of WT and mutant (Gly181Val) enzyme at the expected relative mass of 32 kDa (Supplementary Material, Fig. S2). However, additional bands were observed in the Gly181Val RDH5 samples (Supplementary Material, Fig. S2), probably reflecting degraded and/or misfolded protein arising

from mutation-associated conformational instability (Supplementary Material, Fig. S2). The reactions were performed in the reductive direction for practical reasons related to retinoid stability and extractability. However, RDH-catalyzed reactions are fully reversible (i.e.  $\delta G^\circ \sim 0$  kcal/mol), the direction being determined by the ratio of reduced to oxidized co-substrate, so that the directionality used *in vitro* is immaterial. The activity assays performed with 11-cis-retinal and NADH as substrates showed that the WT enzyme catalyzed formation of 11-cis-retinol product (Fig. 2D). In contrast, no such product was formed by the Gly181Val RDH5 mutant demonstrating that the mutation abolishes catalytic activity (Fig. 2D). Similar expression (Supplementary Material, Fig. S2) and activity (Supplementary Material, Fig. S3) patterns were observed for WT and Gly181Val HsRDH5 suggesting that the pathogenic effect of the mutation is not specific to FcRDH5. From these results, we conclude that any FcRDH5 that may have escaped detection by the immunohistochemical studies shown in Figure 2 is not catalytically active making the Gly181Val substitution a true null mutation.

#### Accumulation of 13-cis-retinoids in RPE of Gly181Val mutant cats

To investigate potential retinoid content changes in mutant cats because of deficient 11-cis-RDH activity, retina and RPE from the eyes of overnight dark-adapted WT ( $RDH5^{+/+}$ ), heterozygous mutant ( $RDH5^{+/-}$ ) and homozygous mutant ( $RDH5^{-/-}$ ) cats were collected, and retinoids extracted for high-performance liquid chromatography (HPLC) analysis (Fig. 3 and Supplementary Material, Fig. S4). Significant levels of cis-retinyl esters, particularly the 13-cis form (peak 1 with  $\lambda_{max}$  of 328 nm in Fig. 3) accumulated in the RPE of the  $RDH5^{-/-}$  cats. The cis-retinyl esters were also found in the RPE of the  $RDH5^{+/-}$  cats, albeit in relatively smaller amounts. However, these cis-esters were absent in the RPE of  $RDH5^{+/+}$  cats. On the other hand, peaks corresponding to all-trans-retinyl esters were present in the RPE samples from  $RDH5^{-/-}$ ,  $RDH5^{+/-}$  and  $RDH5^{+/+}$ . A shoulder peak adjacent to 11-cis-retinol corresponding to 13-cis-retinol was observed in the RPE of  $RDH5^{-/-}$  cats but not in the RPE of the heterozygous and WT cats. The identity of all retinoids was confirmed by comparing elution times with corresponding standards (Supplementary Material, Figs. S5 and S6). The accumulation of 13-cis-retinoids in the homozygous mutant cats resembles findings from studies conducted in  $Rdh5^{-/-}$  mice (10). Although 13-cis-retinoids were also detected in the retina samples, this is possibly because of cross-contamination arising during the dissection of the tissues (Supplementary Material, Fig. S7). Levels of 11-cis-retinal in retina samples of  $RDH5^{-/-}$  cats following extended dark adaptation were comparable to those from  $RDH5^{+/+}$ ,  $RDH5^{+/-}$ , indicating that alternative, but apparently less efficient, pathways exist for oxidation of 11-cis-retinol into 11-cis-retinal. These data are consistent with findings in humans and other model systems that RDH5-deficiency does

not cause a complete metabolic blockade in the visual cycle. Another notable observation was an increase in levels of all-trans-retinal oximes (*syn*- and *anti*-) in the retina samples from  $RDH5^{-/-}$  cats relative to WT and heterozygous cats, although the cause is unclear.

#### Variability of the area centralis degeneration in $RDH5^{-/-}$ cats

As the  $RDH5$  cat colony was expanded and all animals genotyped for the  $RDH5$  Gly181Val pathogenic variant, it became apparent that there was considerable variability in the onset of fundus changes. Most cats showed *area centralis* lesions as juveniles, but a subset lacked such changes. Of 14 cats in the colony homozygous for  $RDH5$ -Gly181Val mutation that were followed up to 2.5 years, 3 had very early onset of *area centralis*/visual streak changes with hyporeflexive lesions developing from 5 months of age followed by thinning in the *area centralis*. Seven cats had similar lesions that developed by 2 years of age but at that age had not progressed to retinal thinning and the final three cats did not develop lesions when followed up to 2.5 years of age (Fig. 4 and Supplementary Material, Fig. S1). This was despite the colony being housed in the same facility and fed the same commercial cat diet suggesting genetic modifying loci were likely responsible. However, all homozygous mutant cats showed the slow recovery of rod function following light exposure as aforementioned. Importantly, none of the cats heterozygous for the mutation or WT cats within the colony developed the characteristic retinal lesions or had a slow recovery of rod function.

#### Macular atrophy in human $RDH5$ -retinopathy subjects

A review of the database of patients with inherited retinal disease at Moorfields Eye Hospital London and The Hospital for Sick Children Toronto identified 17 patients with confirmed biallelic mutations in  $RDH5$ . Of these, seven patients (from six families) had macular atrophy evident on SD-OCT and/or fundus autofluorescence imaging (Table 1, Fig. 5). One patient had been reported in a previous study (patient P1) [patient 7 in Sergouniotis *et al.* (8)]. There were no signs of macular atrophy on retinal imaging in 9 of the 17 patients, and 1 had incomplete clinical data.

All patients with macular atrophy reported lifelong night vision difficulties, with a deterioration in central vision between age 30 and 52 years (Table 1). Consistent with this, patients with macular atrophy were older [mean age  $51.3 \pm 9.8$  SD years ( $n = 7$ )] than those without atrophy [mean age  $22.8 \pm 13.9$  SD years ( $n = 10$ )] ( $P < 0.001$ , two-tailed *t*-test). Visual acuity in patients with macular atrophy ranged from 6/9 to counting fingers at presentation.

Fundus examination showed multiple white or yellowish dots at the posterior pole (Supplementary Material, Fig. S8), extending to the mid-peripheral retina in six out of the seven patients with macular atrophy and two of

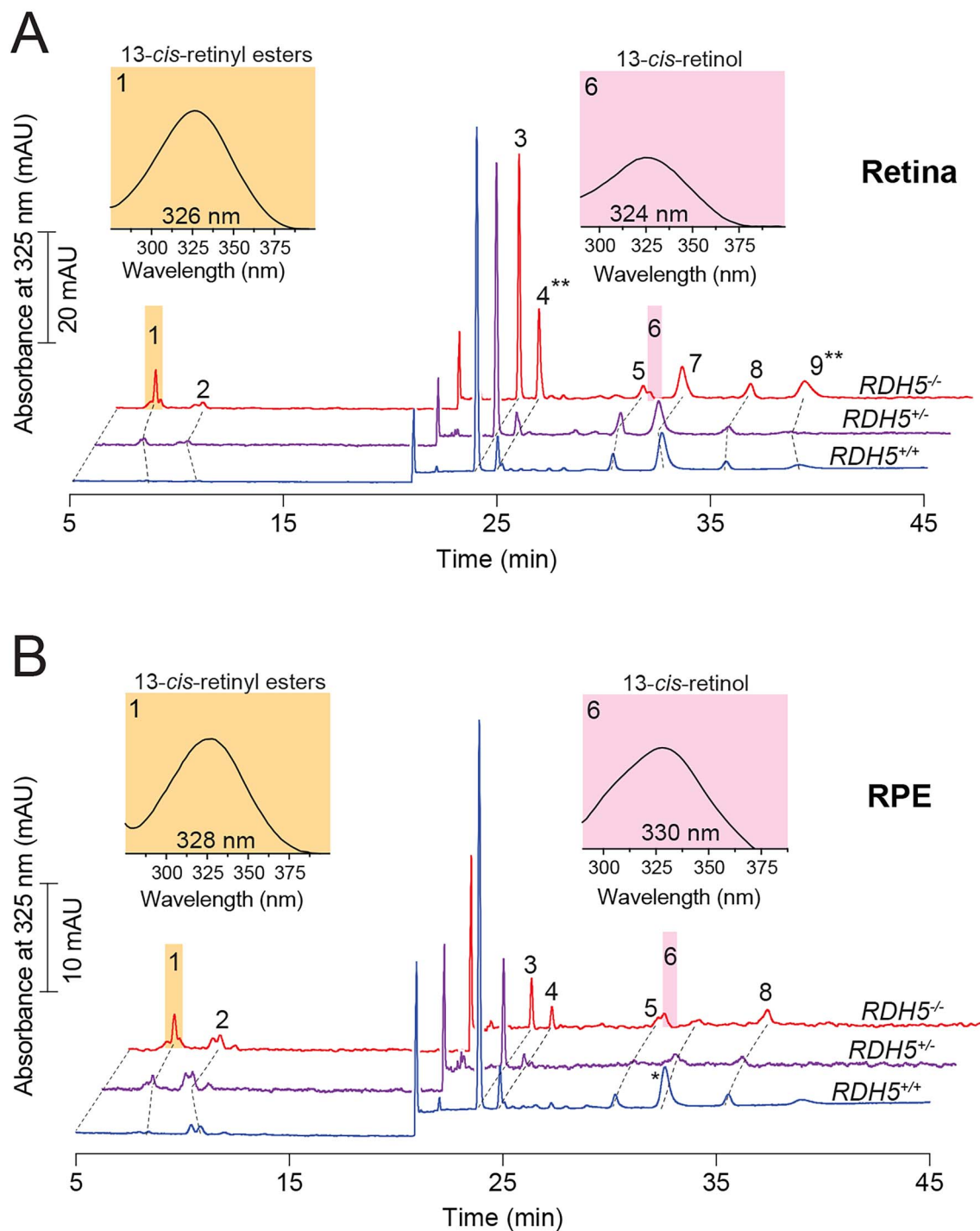


**Figure 3.** Retinoid extraction and analyses from feline retina and RPE samples. Normal phase HPLC elution profiles of retinoids extracted from (A) retina and (B) RPE samples of *RDH5*<sup>+/+</sup> (blue), *RDH5*<sup>+/-</sup> (lavender) and *RDH5*<sup>-/-</sup> (red) cats. Absorbance spectra for 13-cis-retinyl esters (peak 1, yellow-orange) and 13-cis-retinol (peak 6, pink) are shown above their respective peaks. Peak 2, all-trans-retinyl palmitate, peak 3, syn-11-cis-retinal oxime, peak 4, syn-all-trans-retinal oxime, peak 5, 11-cis-retinol, peak 7, anti-11-cis-retinal oxime, peak 8, all-trans-retinol, peak 9, anti-all-trans-retinal oxime. mAU—milli-absorbance units.

these (P3, P7) had a mixed picture of white dots and more generalized peripheral retinal degeneration. P4, the older brother of P3 showed widespread peripheral retinal degeneration with no white dots.

SD-OCT findings ranged from disruption of the ellipsoid zone with perifoveal thinning of the outer nuclear layer (Fig. 5A, D, E, H, Y and AB), to central loss of

the outer nuclear layer (Fig. 5Q, T and U), or widespread outer retinal loss (Fig. 5M and P).

The level of autofluorescence signal was low in all patients as previously reported in this condition (9). Changes in autofluorescence patterns included parafoveal diffuse or annular hypoautofluorescence (Fig. 5B, C, F and K), hyperautofluorescent dots (Fig. 5C),

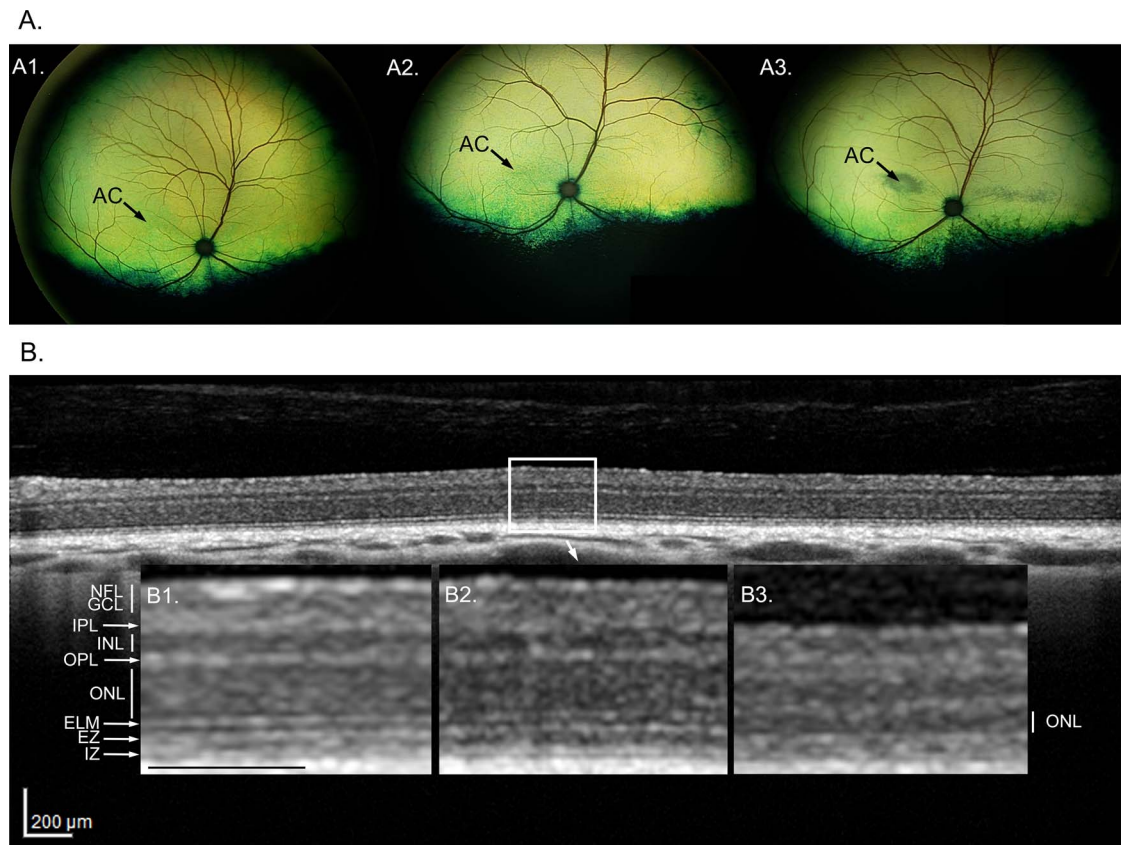


**Figure 4.** Not all  $RDH5^{-/-}$  cats develop *area centralis* degeneration at a young age. **(A)** Wide-angle fundus images of: (A1) WT adult cat; (A2) 2.5-year-old  $RDH5^{-/-}$  cat without *area centralis* degeneration; (A3)  $RDH5^{-/-}$  cat with *area centralis* degeneration. AC = *area centralis* indicated by a black arrow. **(B)** SD-OCT high-resolution cross-sectional images across the *area centralis*. Main image (upper) of a 2.5-year-old  $RDH5^{-/-}$  cat without *area centralis* changes (*area centralis* indicated by a white box). Inset below are magnified view of *area centralis* in: (B1) WT adult cat. (B2) 2.5-year-old  $RDH5^{-/-}$  cat without *area centralis* changes; (B3) 2.5-year-old  $RDH5^{-/-}$  cat with *area centralis* degeneration. Black bar scale in the inset = 200  $\mu\text{m}$ . NFL, nerve fiber layer; GCL, ganglion cell layer; IPL, inner plexiform layer; INL, inner nuclear layer; OPL, outer plexiform layer; ONL, outer nuclear layer; ELM, external limiting membrane; EZ, ellipsoid zone; IZ, interdigitation zone.

central areas of confluent hypofluorescence (Fig. 5R and S) or generalized retinal atrophy including the macular region with widespread loss of autofluorescence (with only autofluorescent signal from the sclera being evident) (Fig. 5N and O).

Serial images were available from three of the seven patients with macular atrophy over a follow-up interval of 7–12 years (Supplementary Material, Fig. S9). Three eyes of these three patients showed progression of macular atrophy over time (Supplementary Material, Fig. S9G–I) and one demonstrated progression of peripheral retinal degeneration (Supplementary Material, Fig. S9E and F). Patient 7 at presentation (44 years) showed a few perifoveal dots that corresponded to hyperreflective deposits at the RPE and associated localized disruptions of outer segment and ellipsoid zone; at 53 years, she had prominent peri-foveal atrophy of outer segment and ellipsoid zone.

ERG was performed in five of the seven patients (summarized in Table 1). In all five, dark-adapted and light-adapted full-field ERGs were subnormal. In one case, ERGs were recorded following prolonged dark adaptation and showed recovery of rod function. In another case, there was minimal difference in responses following standard versus prolonged dark adaptation. The

pattern ERG, which is used to assess macular function, was undetectable in all four patients tested.

### **In vitro activity of human $RDH5$ mutations associated with macular atrophy**

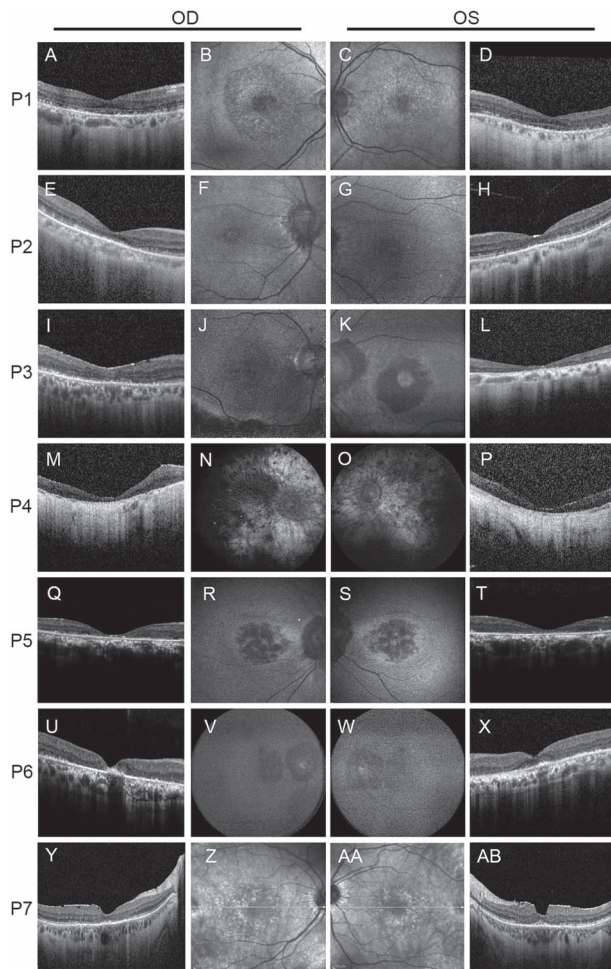
To assess whether the development of macular atrophy was associated with more functionally deleterious mutations, the *in vitro* catalytic activity of three of the  $RDH5$  mutants in the patients with macular atrophy (Table 1), Met253Arg, Ser201Phe and Arg209Ter (Fig. 6A) was assessed. All three mutations have been previously reported in literature, although there has been no prior report of their *in vitro* activity (9,22,31). Recombinant WT and mutant  $RDH5$  proteins with C-terminal 1D4 tags were expressed in Sf9 insect cells and the membrane fractions containing  $RDH5$  were isolated for activity assays (31). An anti-1D4 immunoblot confirmed that the proteins expressed predominantly at the expected molecular size (Supplementary Material, Fig. S10). Activity assays were performed using 11-cis-retinal and NADH as described above for the Fc $RDH5$  constructs. (2). Ser201Phe and Arg209\* were both inactive as exhibited by the lack of an 11-cis-retinol product peak in the HPLC traces (Fig. 3B). Interestingly, Met253Arg  $RDH5$  retains catalytic activity



Table 1. Human subjects' details

Patient	Gender	Ethnicity	At presentation			Symptoms at presentation	At last follow up			Base change	AA change	Electrodiagnostic tests
			Age	VA RE	VA LE		Age	VA RE	VA LE			
1	M	European	55	6/9	2/60 amblyopic	Longstanding night vision problems, central vision worse since age 52	64	2/60	1/60 amblyopic	c.346G > C c.710A > C	p.Gly116Arg p.Tyr237Ser	DA0.01 ERG undetectable; DA10 ERG a and b-waves subnormal with a reduced b:a ratio. Borderline LA 30 Hz and LA 3 ERG amplitudes. DA ERGs normalized after overnight DA. PERG undetectable and central multifocal ERGs reduced bilaterally. Not done
2	F	South Asian	49	6/18	6/18	Life long night blindness, recent reduction in acuity					p.Arg167His p.Trp226Ter	
3*	M	South Asian	55	6/9	2/60	Early onset night blindness, left eye macular hole noted at age 46	67	6/24	1/60	c.33 + 2dup c.758 T > G	p.Met253Arg	DA0.01 ERG severely subnormal DA10 ERG a and b-waves subnormal with a reduced b:a ratio. LA 30 Hz & LA3 ERG a- and b-waves delayed and markedly subnormal with a low LA3 ERG b:a ratio. PERG undetectable and widespread mfERG reduction bilaterally. Not done
4*	M	South Asian	63	CF	CF	Reported night and central vision deteriorated around age 50	77	CF	PL	c.33 + 2dup c.758 T > G	p.Met253Arg	
5	M	South Asian	34	6/12	6/9	Night vision problems in childhood, deterioration of central vision around age 30	45	2/60	1/60	c.602C > T (homozygous)	p.Ser201Phe	DA0.01 ERG subnormal DA10 ERG a and b-waves subnormal with a preserved b:a ratio. LA 30 Hz & LA3 ERG a- and b-waves delayed and markedly subnormal with a low LA3 ERG b:a ratio. PERG undetectable bilaterally.
6	M	South Asian	59	2/60	6/12	Longstanding nyctalopia, reduced central vision around age 43				c.602C > T (homozygous)	p.Ser201Phe	Rod ERG undetectable, bright flash ERG a waves markedly abnormal with reduced b:a ratio. Photopic 30 Hz flicker markedly delayed and subnormal, pattern ERG undetectable.
7	F	European	44	6/6	6/6	Long standing nyctalopia	54	20/40	20/32	c.625c > T (homozygous)	p.Arg209*	Rod ERG moderately reduced, standard flash ERG a-waves markedly reduced and b-waves moderately reduced. Single flash cone and 30 Hz flicker responses are delayed and showed reduced amplitudes.

\*Patients 3 and 4 are siblings. VA: visual acuity, RE: right eye, LE: left eye.



**Figure 5.** Fundus autofluorescence and SD-OCT images of patients with biallelic RDH5 variants and macular atrophy. SD-OCT images (left and right hand columns) and autofluorescence images (central columns) illustrating clinical phenotype in these patients, ranging from relatively localized perifoveal changes (A–D, Y–AB) to widespread retinal atrophy (M–P). In the lowest panels, the central images (Z, AA) show infrared reflectance images. P3 and P4 are siblings.

as seen by the presence of 11-*cis*-retinol in the HPLC chromatogram similar to that observed with the WT enzyme (Fig. 6B). To more precisely examine the catalytic efficiency of Met253Arg in comparison to WT RDH5, steady-state kinetic analysis of both proteins was performed. Reactions with Met253Arg displayed a reduced maximal velocity ( $V_{max}$ ) (1.8 pmol/min/ $\mu$ g) compared with WT enzyme (98.5 pmol/min/mg). However, the Michaelis constant ( $K_m$ ) (88.1  $\mu$ M) was comparable to that of the WT enzyme (65.2  $\mu$ M). Hence, the catalytic efficiency ( $V_{max}/K_m$ ) was reduced 74-fold in the Met253Arg mutant RDH5 relative to the WT protein (Fig. 6C).

To study the putative effects of these mutations at the tertiary structural level, a homology model of dimeric HsRDH5 was created (Fig. 6A). Met253 is located away from the catalytic core and nucleotide binding motif, near the surface of the protein. Substitution to a positively charged Arg residues not only results in a bulkier side chain that introduces steric clashes with nearby residues but also likely disrupts hydrophobic

interactions given the charged nature of the side chain of this residue. From observations on the basis of the substrate binding site in the structure of the *Drosophila* photoreceptor dehydrogenase in complex with a phenol ligand (32), Met253 appears to line the substrate entry portal and the protrusion of the Arg side chain at that position could interfere with active site substrate binding. However, given that Met253Arg maintained low-level retinol dehydrogenase activity in *in vitro* assays, the enzyme can evidently accommodate the structural alteration to some extent thus maintaining active site structure. Ser201 is found within the sixth  $\beta$ -strand of the Rossmann-fold of the HsRDH5 model. A substitution to the bulky aromatic Phe residue at that position introduces severe steric clashes that cannot be resolved with rotamer switching. This is predicted to lead to structural distortions interfering with protein folding and membrane localization of the adjoining C terminal region of the enzyme. Arg209Ter results in the translation of a truncated form of the enzyme with the entire C-terminal end missing (region highlighted in Fig. 6A), which is predicted to disrupt enzyme structure, localization and activity as seen in the *in vitro* assay.

The effect of the compound heterozygous mutants, Gly116Arg, Tyr237Ser, Arg167His and Trp226Ter on protein function were assessed on the basis of the RDH5 homology model. The Trp226Ter mutation results in a severely truncated form of RDH5 that is undoubtedly not an active catalyst. Hence, the structural details of this mutant were not considered further.

Substitution of the Gly residue at position 116 with Arg residue results in a major change in the size and charge of the side chain. Although the Arg side chain can orient away from the protein, no rotamer is capable of avoiding steric clashes with nearby residues (Supplementary Material, Fig. S11A) suggesting this substitution would be functionally detrimental. In addition, Gly residues frequently play important roles in protein folding owing to their backbone atom conformational flexibility. As such, the Gly116Arg substitution could negatively impact protein folding or stability.

Tyr237 is located distant from the protein core on a surface helical turn. However, it is positioned with its phenyl ring buried and away from the exterior solvent, hydrogen bonded with the side chain oxygen of Glu216. Substitution to Ser residue at this position similarly results in an uncharged residue but potentially breaks the H-bond with Glu216, although the Ser residue can potentially form a new stabilizing H-bond with Thr333 (Supplementary Material, Fig. S11B). Ser residue is much more solvent exposed than the Tyr residue it replaces. This substitution results in a hydrophobic void that could destabilize the protein or make it aggregation prone.

Arg residue at position 167 is observed to be surface exposed and in proximity to the dimer interface. A mutation to His residue retains the basic nature of the amino acid but leads to a slightly buried rotamer and thus a slight expansion of the surrounding cavity pocket. In addition, the introduction of the imidazole ring

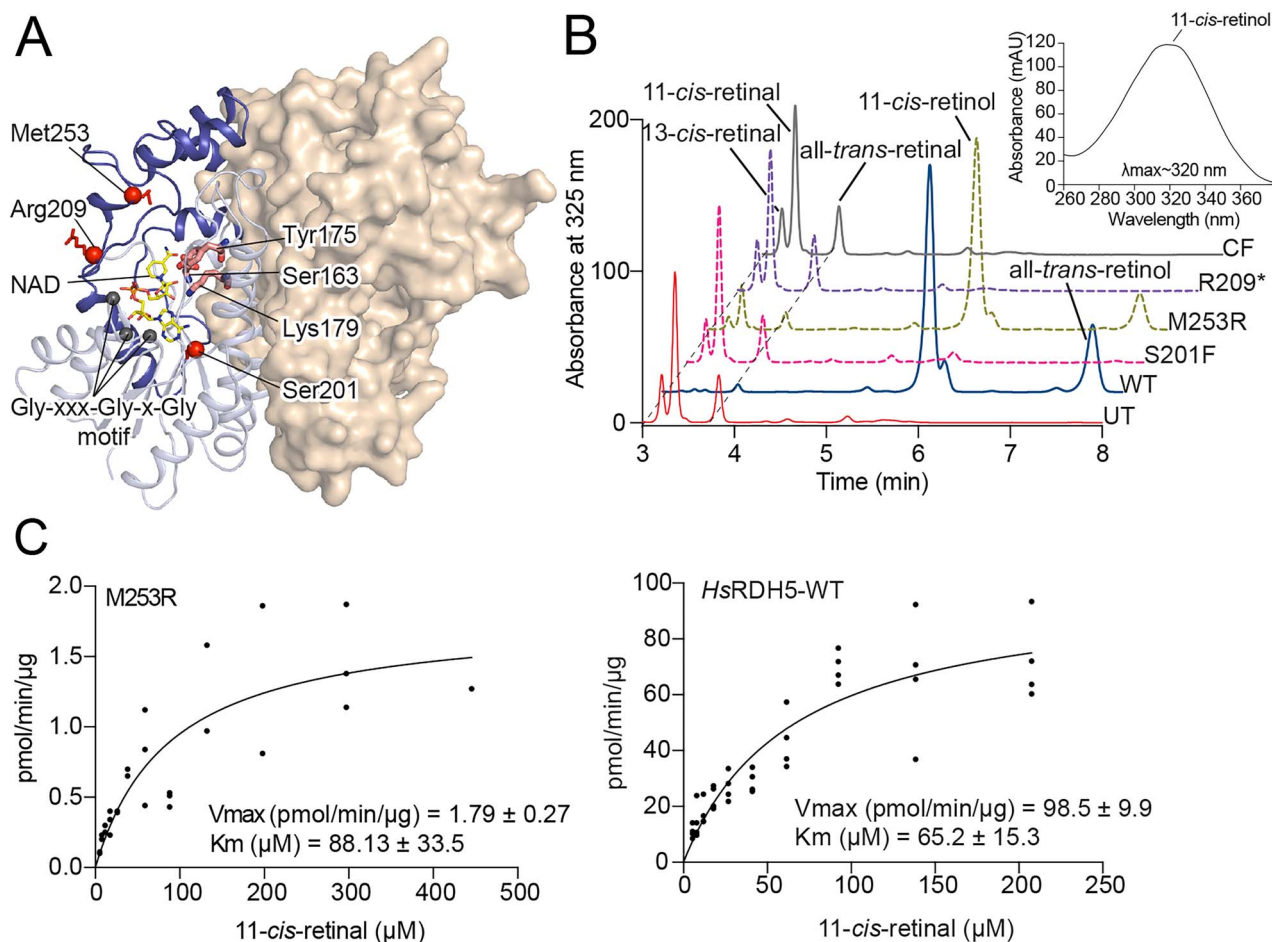


**Figure 6.** Homology model and activity of *H. sapiens* RDH5 WT and its mutants. **(A)** Homology model of dimeric HsRDH5 created using SwissModel. The two monomers are indicated as blue cartoon and wheat colored surface. The region of the cartoon downstream of residue Arg209 is highlighted in a darker shade of blue. All putative mutant residues Ser201, Met253 and Arg209 are shown in red as spheres (C-alphas) with their side chains depicted as lines. The catalytic triad residues Ser163, Tyr175 and Lys179 are highlighted in pink as sticks. C-alphas of co-factor binding motif (Gly-XXX-Gly-X-Gly) residues are highlighted as gray spheres. To the right of A is a 90° rotated view with the nucleotide NAD superimposed in the co-factor binding motif, as a stick (yellow) from the dPDH structure (PDB: 5ilo). **(B)** Shows the normal phase HPLC traces from activity assays of HsRDH5 WT (HsRDH5-WT) and its mutants, HsRDH5-Ser201Phe/Met253Arg/Arg209\*. Retinoid elution profiles from reactions using HsRDH5-WT (blue) and HsRDH5-Met253Arg (green) show near complete conversion of 11-*cis*-retinal to 11-*cis*-retinol, whereas that of the mutants (HsRDH5-S201F, dark pink and HsRDH5-Arg209\*, violet) show near absence of 11-*cis*-retinol formation, indicating loss of dehydrogenase function. Un-transfected (UT) and CellFectin only transfected Sf9 cells were used as controls. Chromatography was performed using an isocratic flow of 80% hexane and 20% ethyl acetate over a period of 10 min. **(C)** Michaelis-Menten steady state kinetics for HsRDH5-Met253Arg using a range of 11-*cis*-retinal concentrations.

of His residue causes a major steric clash with the nearby Glu204 (Supplementary Material, Fig. S11C). This could lead to the disruption of the salt bridge predicted to be formed between the WT Arg residue (-N) and Glu204 (-OE1). In the model, Arg167 also forms an H-bond with Ser282, Glu204 and Trp291. Although a substitution to His residue maintains the bond with Trp291, it breaks the bond with Ser282. It also forms a new H-bond with Glu183. Such reshuffling of bonds could be damaging to protein folding. In addition, the His residue rotamer is noticeably closer to the catalytic residue Ser163, which could have consequential effects on substrate binding and enzyme function.

## Discussion

RDH5 functional impairment reduces the rate of 11-*cis*-retinal regeneration by the classical visual cycle leading to slowed dark adaptation in affected individuals.

Originally considered a stationary condition causing night blindness, it is now recognized that patients with biallelic *RDH5* mutations often develop more serious progressive retinal changes. In addition to slow recovery of rod function, cone dysfunction can develop leading to sight-threatening degenerative changes in the macula, which is the retinal region responsible for high-acuity vision.

## Cat RDH5-retinopathy

The new cat model for *RDH5*-retinopathy reported here has a missense mutation (c.542G > T; p.Gly181Val) that ablates all *RDH5* function when assayed *in vitro*. The mutation is likely to interfere with *RDH5* dimerization and probably affects stability of the protein as *RDH5* could not be detected by either western blot or immunohistochemistry of RPE in homozygous mutant animals. The resulting phenotype of the *RDH5*-Gly181Val

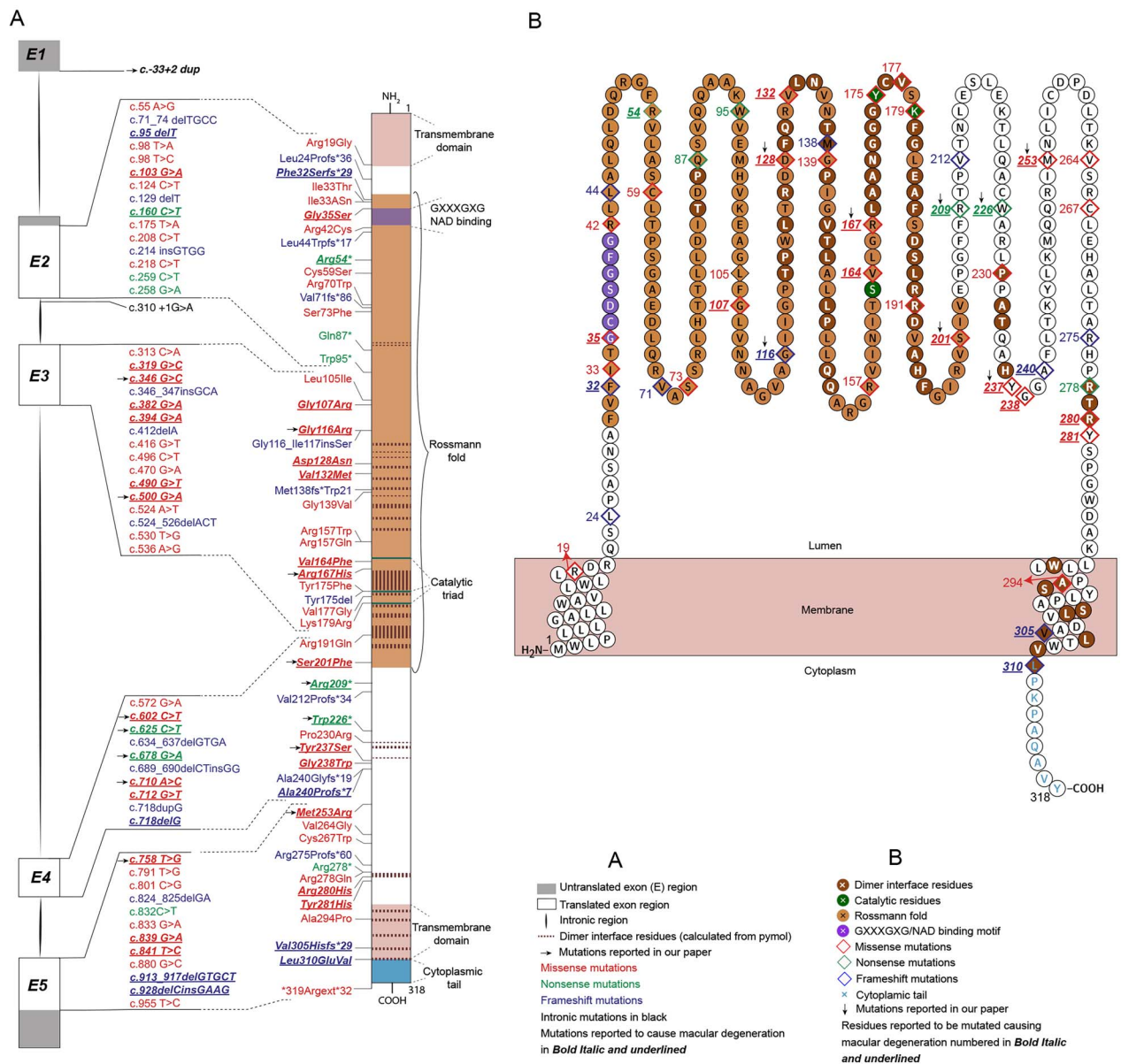


**Figure 7.** Human RDH5 gene and amino acid mutations. **(A)** The exon–intron organization of the *H. sapiens* RDH5 gene, adapted from NCBI (Gene ID: 5959), mapped from position 55 720 393 to 55 724 705 bps on chromosome 12. The 5' upstream and 3' downstream flanking sequences have not been included for simplification. Translated exon regions (E2–E5) are shown in white, untranslated exon regions (E1, part of E2 and E5) are shown in gray along with intronic regions as black lines. Mutations in the coding exonic sequences are shown to the right of each exon in ascending order (demarcated with black lines) and colored according to mutation type—missense (red), frameshift (blue) and nonsense (green). The mutations occurring in the introns are numbered in relation to the coding exon sequences and highlighted in black. The polypeptide bar diagram (N terminus to C terminus, top to bottom) is drawn on the right in A, highlighting all the functional domains and motifs (labeled in figure). Resultant mutations in the amino acid sequence are shown to the left of the bar diagram (demarcated with black dotted lines —); color coordinated to their respective exon mutations with their location marked on the polypeptide. **(B)** The 2D transmembrane topology of the RDH5 polypeptide as generated using the webserver, Protter (51) on the basis of information from UniProt. Residues reported to be mutated are numbered and colored according to mutation type as mentioned in A. Color representations of the residues that are part of functional domains/motifs are shown in legend alongside the figure and are matched to the corresponding region on the polypeptide bar diagram in A (A and B). All mutations reported to be associated with macular changes are highlighted in bold italic and underlined (including those in the current study). Amino acid mutations reported in the current study are also marked with a black arrow (→/↓).

cat recapitulates several major aspects of human RDH5-retinopathy. Affected cats all show a very marked delay in recovery of rod function following light exposure, a feature that distinguishes this cat model from the *Rdh5*<sup>-/-</sup> mouse in which slowed dark adaptation was observed only when extremely intense light exposure was used for photobleaching experiments (10). These cats also develop the equivalent of a macular atrophy.

Laboratory rodents do not have a similar high-acuity retinal region (33) and therefore are not suitable to model macular atrophy.

The earliest indication of photoreceptor structural change in the *area centralis* and visual streak of affected cats is the elongation and distortion of photoreceptor outer segments. This causes hyporeflexive lesions seen by funduscopy and cSLO. With progression,

photoreceptor degeneration follows in the *area centralis*. Although the *area centralis* has a higher density of cones than the peripheral retina, rods still outnumber cones by ~10:1 (34). Considering the degree of thinning that develops, it is clear that substantial rod degeneration occurs in the affected cats. However, further studies are required to assess the extent and dynamics of cone loss. Some cats develop early retinal degenerative changes (from as young as 5 months of age), whereas others have a much later development of these changes with some not showing any changes to at least 2.5 years of age. The latter category of cats will need to be followed for several years to see whether they develop *area centralis* degeneration as they age. The RDH5-Gly181Val cats are housed in a single colony with identical feeding and housing, suggesting that environmental factors are unlikely contributors to phenotypic variability. Thus, it appears more likely that inherited modifying loci play a significant role in defining phenotype, as has been suggested in several studies of human subjects with RDH5-associated retinopathy (20,23,24). Further cross breeding of the cat colony is underway to investigate the inheritance of the putative modifying factor(s).

The feature of RDH5-retinopathy that is not manifested in the RDH5-Gly181Val cat is the development of white dots in the retina that are a striking ophthalmoscopic feature of the condition in humans. Development of retinal white dots is not unique to RDH5-retinopathy and can also be seen in patients with mutations in other visual cycle genes and in vitamin A deficiency (35). The anatomical position of the fundus white dots has been characterized by OCT imaging, but their composition remains the subject of speculation. The lack of white dot formation in the RDH5 mutant cat could be accounted for by species differences in retinoid levels or metabolism. RPE samples from the RDH5 mutant cats have an accumulation of 13-*cis* retinoids, which is similar to the findings reported in *Rdh5*<sup>-/-</sup> mice (10). However, it is not known how this compares to the situation in human patients.

Understanding the molecular mechanisms that place the *area centralis* (cat) or macula (human) at risk for degeneration in the face of limited supply of retinoid could suggest pathways to preserve the macula in patients not only with RDH5 mutations but with other macular disease.

### Human RDH5-retinopathy

Progressive degenerative retinal changes, including macular atrophy, are being more commonly recognized in subjects with biallelic RDH5 mutations. Early changes can be detected by the use of higher resolution imaging, which is becoming more widely used to investigate patients with RDH5-associated retinopathy. For example, studies utilizing adaptive-optics imaging have shown reductions in cone numbers even where no lesions can be detected on regular fundus examination (11,36). The seven human subjects in the current study had

between them a total of eight different RDH5 mutations. The c.678G > A; p.Trp226\* identified in patient 2 has not been previously reported in the literature, whereas the remaining seven mutations have been described previously. A total of 56 different RDH5 mutations are currently reported in the literature (Fig. 7 and Supplementary Material, Table S3), 21 of which have been reported to be associated with macular changes (highlighted in Fig. 7 and shown with ages for patients homozygous for variants in Supplementary Material, Table S3).

The risk of patients with RDH5 mutations developing macular atrophy increases with age. However, a wide range of ages have been reported for the development of macular atrophy with the youngest being a 9-year-old patient (21). It seems reasonable to hypothesize that mutations that cause complete loss of function could be more frequently associated with macular atrophy. Indeed, the mutations examined in this study from patients with macular disease were found or predicted to cause either severe or complete loss of function. However, this does not appear to completely explain the phenotype differences. The *in vitro* assay of enzymatic function of the Met253Arg mutation showed low-level residual function that was nevertheless insufficient to prevent the development of macular degeneration (patients P3 and P4). In a report of a family with three members homozygous for the same mutation, a 45-year-old was reported to have macular degeneration, whereas a 10- and 17-year-old had no macular changes suggesting the influence of age (22). The other mutations we report in this study were either shown by *in vitro* assays to ablate RDH5 function (Ser201Phe and Arg209\*) or were confidently predicted to ablate function. P5 and P6 in this study were homozygous for the Ser201Phe RDH5 mutation and three additional patients homozygous for this mutation (ages from 15 to 25) have been reported (30,37), all of which developed macular degeneration (Supplementary Material, Table S3). P7 in this study was homozygous for the Arg209\* mutation and developed progressive macular atrophy as followed from 44 to 54 years of age, and one other patient homozygous for this variant is reported, who at 34 years of age did not show macular atrophy (9). Within-family variations of phenotype have been described. For example, Hotta *et al.* (23) reported on a consanguineous family with siblings homozygous for a Gly107Arg RDH5 mutation where the brother (56 years of age) had bilateral macular atrophy, whereas his 51-year-old sister had cone dysfunction but with almost normal appearing maculae on the basis of ophthalmoscopy. The studies from Katagiri *et al.* (20) of 25 patients and Pras *et al.* (24) of 22 patients both reported a lack of consistent genotype–phenotype correlation and suggested a possible influence of environmental factors or variants in modifier genes as explanations for the variability in severity of disease phenotype.

An exon 5 indel (c.928delCinsGAAG; p.Leu310GluVal) is a common cause of RDH5-retinopathy in Japanese

patients. Liden *et al.* (3) showed the mutation reduced *in vivo* activity to 1.7% of normal and that in an *in vitro* assay there was no activity. There are 41 patients reported homozygous for this mutation (27 males and 14 females) (16,18,20,36,38–42) where 10 were reported to have macular atrophy (9 males and 1 female) with a mean age of 57 years (range 40–78 years) and 31 were not reported to have macular atrophy (18 males and 13 females) with a mean age of 31.8 years (range 6–66 years). The reason for the apparent sex disparity is not known.

Missense mutations comprise the commonest category of *RDH5* disease causing (61%) followed by those predicted to result in premature termination codons (nonsense or frameshift mutations) (34%) (Fig. 7). The proportion of different classes of mutation in patients with macular degeneration is very similar to the overall proportions (missense: 61% vs. 62% and premature termination 34% vs. 33% for all patients compared with patients with reported macular phenotypes). Mutations occur along the entire length of the gene affecting all domains of tertiary structure. Major protein regions include the Rossmann-fold (residue 30–203) and a second lumen region (204–288). An analysis as to whether mutations associated with macular phenotypes were associated more with one or other of these regions compared with all mutations showed no association (Fisher's Exact test  $P = 0.21$ ). Therefore, it appears that although age is a risk factor for macular involvement, type of gene mutation and position along the protein are not major contributors to risk and that there are other important factors such as background genetics.

### Future prospects

Some therapeutic approaches to protect from macular atrophy use RPE65 inhibitors to slow down the visual cycle (43). Achieving a balance between protective effects and deleterious effects from inhibition of the visual cycle could be further investigated using this cat model. Currently, there is no effective treatment to prevent progression of visual impairment with *RDH5*-associated retinopathy, although oral dosing with 9-*cis*- $\beta$ -carotene has been shown to improve visual fields and recovery of rod dark adaptation (44). The cat model could also be used to screen candidate therapies including translatable gene augmentation therapy.

In summary, the similarities between the *RDH5*-Gly181Val cat model and human *RDH5*-retinopathies mean that the cat is a valuable and much-needed model that can help in the understanding of *RDH5*-associated retinal dysfunction and degeneration and for testing potential therapeutic interventions.

## Materials and Methods

### Feline phenotypic studies

A breeding colony was established following identification of a single male cat with abnormal retinal changes affecting the *area centralis* and visual streak. This animal

was crossed with phenotypically normal female cats and some F1 females backcrossed with the proband developed. Animals in these litters developed the same fundus changes (a partial pedigree shown in [Supplementary Material, Fig. S1](#)). Further backcrossing and crossing between litters were performed to further expand the colony to provide additional animals to study. This supported a recessive mode of inheritance.

Phenotyping studies were as described previously (45) and details are provided in [Supplementary Methods](#).

### Feline genetic studies

WGS of cats was performed on a trio of cats: two affected and one obligate carrier (animals indicated on pedigree [Supplementary Material, Fig. S1](#)) was performed as part of the 99 Lives Cat Genome Sequencing Initiative (<http://felinegenetics.missouri.edu/99lives>), as previously described (46). Details are provided in S1 Appendix. Candidate variants identified by WGS were genotyped in colony animals by polymerase chain reaction (PCR) amplification and Sanger sequencing. The variants and PCR primers are listed in [Supplementary Material, Table S1](#).

### In vitro expression and activity assays

cDNAs encoding WT and Gly181Val *F. catus* and WT *Homo sapiens* *RDH5* and Hs*RDH5* mutants Ser201Phe, Met253Arg and Arg209\* were generated. The WT and mutant *RDH5* clones were expressed in insect cells and the purified proteins used in a previously described assay system employing normal phase HPLC to quantify the formation of 11-*cis*-retinol from 11-*cis*-retinal substrate (27). Details are provided in [Supplementary Methods](#).

### Extraction and analysis of retinoids from feline eyes

Retinoids were extracted from ocular tissues of cats that had been dark-adapted overnight. Retinoids were extracted and separated on a normal phase HPLC column using the protocol described in Choi *et al.* (47). Details are provided in S1 Appendix. Immunoblotting of feline retinal and RPE samples used for retinoid analysis was also performed. Details and antibodies are provided in [Supplementary Methods](#).

### Homology model of feline and human *RDH5*

Homology models of Fc*RDH5* and Hs*RDH5* were generated using the SwissModel online protein structure homology-modeling server (48). Details are provided in [Supplementary Methods](#).

### Study approval

The human patient part of the study was approved by Moorfields Eye Hospital and Northwest London Research Ethics Committee and REB of Hospital for Sick Children, Toronto and conformed to the tenets of the Declaration of Helsinki. All patients provided written informed consent. The feline studies were performed in accordance

with the Association for Research in Vision and Ophthalmology statement for the Use of Animals in Ophthalmic and Vision Research and approved by the Michigan State University Institutional Animal Care and Use Committee (approved protocols: 05–11–106-00, 05–14–090-00, 05–17–075-00, PROTO202000013).

## Human subjects

Retinal degeneration patients at Moorfields Eye Hospital London and The Hospital for Sick Children Toronto with biallelic variants in *RDH5* were identified. Those with macular atrophy were included in this study. Patient details are included in [Table 1](#). Details are provided in [Supplementary Methods](#).

## Supplementary Material

[Supplementary Material](#) is available at [HMG online](#).

*Conflict of Interest statement.* None declared.

## Funding

The views expressed are those of the authors and not the funding organizations. MSU Endowed Research Funds, Morris Animal Foundation and Myers-Dunlap Endowment (to S.P.J.); Department of Veterans Affairs (I01BX004939 to P.D.K.); the National Institutes of Health (R24EY027283 to K.P., P.D.K., S.P.J.); an unrestricted grant from Research to Prevent Blindness to the Department of Ophthalmology at University of California, Irvine (to A.D., K.P., P.D.K.); Foundation Fighting Blindness USA (CD-CL-0617-0727-HSC to A.V.); Wellcome Trust (206619\_Z\_17\_Z); National Institute of Health Research Biomedical Research Centre at Moorfields Eye Hospital; UCL Institute of Ophthalmology, London.

## References

- Daruwalla, A., Choi, E.H., Palczewski, K. and Kiser, P.D. (2018) Structural biology of 11-cis-retinaldehyde production in the classical visual cycle. *Biochem. J.*, **475**, 3171–3188.
- Simon, A., Hellman, U., Wernstedt, C. and Eriksson, U. (1995) The retinal pigment epithelial-specific 11-cis retinol dehydrogenase belongs to the family of short chain alcohol dehydrogenases. *J. Biol. Chem.*, **270**, 1107–1112.
- Liden, M., Romert, A., Tryggvason, K., Persson, B. and Eriksson, U. (2001) Biochemical defects in 11-cis-retinol dehydrogenase mutants associated with fundus albipunctatus. *J. Biol. Chem.*, **276**, 49251–49257.
- Cideciyan, A.V., Haeseleer, F., Fariss, R.N., Aleman, T.S., Jang, G.F., Verlinde, C., Marmor, M.F., Jacobson, S.G. and Palczewski, K. (2000) Rod and cone visual cycle consequences of a null mutation in the 11-cis-retinol dehydrogenase gene in man. *Vis. Neurosci.*, **17**, 667–678.
- Gonzalez-Fernandez, F., Kurz, D., Bao, Y., Newman, S., Conway, B.P., Young, J.E., Han, D.P. and Khani, S.C. (1999) 11-cis retinol dehydrogenase mutations as a major cause of the congenital night-blindness disorder known as fundus albipunctatus. *Mol. Vis.*, **5**, 41.
- Yamamoto, H., Simon, A., Eriksson, U., Harris, E., Berson, E.L. and Dryja, T.P. (1999) Mutations in the gene encoding 11-cis retinol dehydrogenase cause delayed dark adaptation and fundus albipunctatus. *Nat. Genet.*, **22**, 188–191.
- Querques, G., Carrillo, P., Querques, L., Bux, A.V., Del Curatolo, M.V. and Delle Noci, N. (2009) High-definition optical coherence tomographic visualization of photoreceptor layer and retinal flecks in fundus albipunctatus associated with cone dystrophy. *Arch. Ophthalmol.*, **127**, 703–706.
- Sergouniotis, P.I., Sohn, E.H., Li, Z., McBain, V.A., Wright, G.A., Moore, A.T., Robson, A.G., Holder, G.E. and Webster, A.R. (2011) Phenotypic variability in *RDH5* retinopathy (fundus albipunctatus). *Ophthalmology*, **118**, 1661–1670.
- Schatz, P., Preising, M., Lorenz, B., Sander, B., Larsen, M., Eckstein, C. and Rosenberg, T. (2010) Lack of autofluorescence in fundus albipunctatus associated with mutations in *RDH5*. *Retina*, **30**, 1704–1713.
- Driessen, C.A., Winkens, H.J., Hoffmann, K., Kuhlmann, L.D., Janssen, B.P., Van Vugt, A.H., Van Hooser, J.P., Wieringa, B.E., Deutman, A.F., Palczewski, K. et al. (2000) Disruption of the 11-cis-retinol dehydrogenase gene leads to accumulation of cis-retinols and cis-retinyl esters. *Mol. Cell. Biol.*, **20**, 4275–4287.
- Song, H., Latchney, L., Williams, D. and Chung, M. (2014) Fluorescence adaptive optics scanning laser ophthalmoscope for detection of reduced cones and hypoautofluorescent spots in fundus albipunctatus. *JAMA Ophthalmol.*, **132**, 1099–1104.
- Yamamoto, H., Yakushijin, K., Kusuhara, S., Escano, M.F., Nagai, A. and Negi, A. (2003) A novel *RDH5* gene mutation in a patient with fundus albipunctatus presenting with macular atrophy and fading white dots. *Am. J. Ophthalmol.*, **136**, 572–574.
- Wang, N.K., Chuang, L.H., Lai, C.C., Chou, C.L., Chu, H.Y., Yeung, L., Chen, Y.P., Chen, K.J., Wu, W.C., Chen, T.L. et al. (2012) Multimodal fundus imaging in fundus albipunctatus with *RDH5* mutation: a newly identified compound heterozygous mutation and review of the literature. *Doc. Ophthalmol.*, **125**, 51–62.
- Kuehlewein, L., Nasser, F., Gloeckle, N., Kohl, S. and Zrenner, E. (2017) Fundus albipunctatus associated with cone dysfunction. *Retin. Cases Br. Rep.*, **11**(Suppl 1), S73–S76.
- Miyake, Y., Shiroyama, N., Sugita, S., Horiguchi, M. and Yagasaki, K. (1992) Fundus albipunctatus associated with cone dystrophy. *Br. J. Ophthalmol.*, **76**, 375–379.
- Nakamura, M., Hotta, Y., Tanikawa, A., Terasaki, H. and Miyake, Y. (2000) A high association with cone dystrophy in fundus albipunctatus caused by mutations of the *RDH5* gene. *Invest. Ophthalmol. Vis. Sci.*, **41**, 3925–3932.
- Nakamura, M., Lin, J. and Miyake, Y. (2004) Young monozygotic twin sisters with fundus albipunctatus and cone dystrophy. *Arch. Ophthalmol.*, **122**, 1203–1207.
- Nakamura, M., Skalet, J. and Miyake, Y. (2003) *RDH5* gene mutations and electroretinogram in fundus albipunctatus with or without macular dystrophy: *RDH5* mutations and ERG in fundus albipunctatus. *Doc. Ophthalmol.*, **107**, 3–11.
- Ruther, K., Janssen, B.P., Kellner, U., Janssen, J.J., Bohne, M., Reimann, J. and Driessen, C.A. (2004) Clinical and genetic findings in a patient with fundus albipunctatus. *Ophthalmologie*, **101**, 177–185.
- Katagiri, S., Hayashi, T., Nakamura, M., Mizobuchi, K., Gekka, T., Komori, S., Ueno, S., Terasaki, H., Sakuramoto, H., Kuniyoshi, K. et al. (2020) *RDH5*-related fundus albipunctatus in a large Japanese cohort. *Invest. Ophthalmol. Vis. Sci.*, **61**, 53.
- Nakamura, M. and Miyake, Y. (2002) Macular dystrophy in a 9-year-old boy with fundus albipunctatus. *Am. J. Ophthalmol.*, **133**, 278–280.

22. Ajmal, M., Khan, M.I., Neveling, K., Khan, Y.M., Ali, S.H., Ahmed, W., Iqbal, M.S., Azam, M., den Hollander, A.I., Collin, R.W. et al. (2012) Novel mutations in RDH5 cause fundus albipunctatus in two consanguineous Pakistani families. *Mol. Vis.*, **18**, 1558–1571.
23. Hotta, K., Nakamura, M., Kondo, M., Ito, S., Terasaki, H., Miyake, Y. and Hida, T. (2003) Macular dystrophy in a Japanese family with fundus albipunctatus. *Am. J. Ophthalmol.*, **135**, 917–919.
24. Pras, E., Pras, E., Reznik-Wolf, H., Sharon, D., Raivech, S., Barkana, Y., Abu-Horowitz, A., Ygal, R. and Banin, E. (2012) Fundus albipunctatus: novel mutations and phenotypic description of Israeli patients. *Mol. Vis.*, **18**, 1712–1718.
25. Shang, E., Lai, K., Packer, A.I., Paik, J., Blaner, W.S., de Moraes Vieira, M., Gouras, P. and Wolgemuth, D.J. (2002) Targeted disruption of the mouse cis-retinol dehydrogenase gene: visual and nonvisual functions. *J. Lipid Res.*, **43**, 590–597.
26. Kim, T.S., Maeda, A., Maeda, T., Heinlein, C., Kedishvili, N., Palczewski, K. and Nelson, P.S. (2005) Delayed dark adaptation in 11-cis-retinol dehydrogenase-deficient mice: a role of RDH11 in visual processes in vivo. *J. Biol. Chem.*, **280**, 8694–8704.
27. Jang, G.F., Van Hooser, J.P., Kuksa, V., McBee, J.K., He, Y.G., Janssen, J.J., Driessen, C.A. and Palczewski, K. (2001) Characterization of a dehydrogenase activity responsible for oxidation of 11-cis-retinol in the retinal pigment epithelium of mice with a disrupted RDH5 gene. A model for the human hereditary disease fundus albipunctatus. *J. Biol. Chem.*, **276**, 32456–32465.
28. Maeda, A., Maeda, T., Sun, W., Zhang, H., Baehr, W. and Palczewski, K. (2007) Redundant and unique roles of retinol dehydrogenases in the mouse retina. *Proc. Natl. Acad. Sci. U. S. A.*, **104**, 19565–19570.
29. Qiu, W., Campbell, R.L., Gangloff, A., Dupuis, P., Boivin, R.P., Tremblay, M.R., Poirier, D. and Lin, S.X. (2002) A concerted, rational design of type 1 17 $\beta$ -hydroxysteroid dehydrogenase inhibitors: estradiol-adenosine hybrids with high affinity. *FASEB J.*, **16**, 1829–1831.
30. Simon, A., Romert, A., Gustafson, A.L., McCaffery, J.M. and Eriksson, U. (1999) Intracellular localization and membrane topology of 11-cis retinol dehydrogenase in the retinal pigment epithelium suggest a compartmentalized synthesis of 11-cis retinaldehyde. *J. Cell Sci.*, **112**, 549–558.
31. Sultan, N., Ali, I., Bukhari, S.A., Baig, S.M., Asif, M., Qasim, M., Naseer, M.I. and Rasool, M. (2018) A novel mutation in RDH5 gene causes retinitis pigmentosa in consanguineous Pakistani family. *Genes Genomics*, **40**, 553–559.
32. Hofmann, L., Tsybovsky, Y., Alexander, N.S., Babino, D., Leung, N.Y., Montell, C., Banerjee, S., von Lintig, J. and Palczewski, K. (2016) Structural insights into the *Drosophila melanogaster* retinol dehydrogenase, a member of the short-chain dehydrogenase/reductase family. *Biochemistry*, **55**, 6545–6557.
33. Linberg, K.A., Lewis, G.P., Shaaw, C., Rex, T.S. and Fisher, S.K. (2001) Distribution of S- and M-cones in normal and experimentally detached cat retina. *J. Comp. Neurol.*, **430**, 343–356.
34. Steinberg, R.H., Reid, M. and Lacy, P.L. (1973) The distribution of rods and cones in the retina of the cat (*Felis domesticus*). *J. Comp. Neurol.*, **148**, 229–248.
35. Khan, K.N., Mahroo, O.A., Khan, R.S., Mohamed, M.D., McKibbin, M., Bird, A., Michaelides, M., Tufail, A. and Moore, A.T. (2016) Differentiating drusen: drusen and drusen-like appearances associated with ageing, age-related macular degeneration, inherited eye disease and other pathological processes. *Prog. Retin. Eye Res.*, **53**, 70–106.
36. Makiyama, Y., Ooto, S., Hangai, M., Ogino, K., Gotoh, N., Oishi, A. and Yoshimura, N. (2014) Cone abnormalities in fundus albipunctatus associated with RDH5 mutations assessed using adaptive optics scanning laser ophthalmoscopy. *Am. J. Ophthalmol.*, **157**(558–570), e551–e554.
37. Eisenberger, T., Neuhaus, C., Khan, A.O., Decker, C., Preising, M.N., Friedburg, C., Bieg, A., Gliem, M., Charbel Issa, P., Holz, F.G. et al. (2013) Increasing the yield in targeted next-generation sequencing by implicating CNV analysis, non-coding exons and the overall variant load: the example of retinal dystrophies. *PLoS One*, **8**, e78496.
38. Liu, X., Liu, L., Li, H., Xu, F., Jiang, R. and Sui, R. (2015) RDH5 retinopathy (fundus albipunctatus) with preserved rod function. *Retina*, **35**, 582–589.
39. Hirose, E., Inoue, Y., Morimura, H., Okamoto, N., Fukuda, M., Yamamoto, S., Fujikado, T. and Tano, Y. (2000) Mutations in the 11-cis retinol dehydrogenase gene in Japanese patients with fundus albipunctatus. *Invest. Ophthalmol. Vis. Sci.*, **41**, 3933–3935.
40. Yang, G., Liu, Z., Xie, S., Li, C., Lv, L., Zhang, M. and Zhao, J. (2017) Genetic and phenotypic characteristics of four Chinese families with fundus albipunctatus. *Sci. Rep.*, **7**, 46285.
41. Wada, Y., Abe, T., Fuse, N. and Tamai, M. (2000) A frequent 1085delC/insGAAG mutation in the RDH5 gene in Japanese patients with fundus albipunctatus. *Invest. Ophthalmol. Vis. Sci.*, **41**, 1894–1897.
42. Niwa, Y., Kondo, M., Ueno, S., Nakamura, M., Terasaki, H. and Miyake, Y. (2005) Cone and rod dysfunction in fundus albipunctatus with RDH5 mutation: an electrophysiological study. *Invest. Ophthalmol. Vis. Sci.*, **46**, 1480–1485.
43. Kiser, P.D., Zhang, J., Badiie, M., Kinoshita, J., Peachey, N.S., Tochtrop, G.P. and Palczewski, K. (2017) Rational tuning of visual cycle modulator pharmacodynamics. *J. Pharmacol. Exp. Ther.*, **362**, 131–145.
44. Rotenstreich, Y., Harats, D., Shaish, A., Pras, E. and Belkin, M. (2010) Treatment of a retinal dystrophy, fundus albipunctatus, with oral 9-cis- $\beta$ -carotene. *Br. J. Ophthalmol.*, **94**, 616–621.
45. Occeili, L.M., Tran, N.M., Narfstrom, K., Chen, S. and Petersen-Jones, S.M. (2016) CrxRdy cat: a large animal model for CRX-associated Leber congenital Amaurosis. *Invest. Ophthalmol. Vis. Sci.*, **57**, 3780–3792.
46. Buckley, R.M., Gandolfi, B., Creighton, E.K., Pyne, C.A., Bouhan, D.M., LeRoy, M.L., Senter, D.A., Gobble, J.R., Abitbol, M., Lyons, L.A. et al. (2020) Werewolf, there Wolf: variants in hairless associated with Hypotrichia and Roaning in the Lykoi cat breed. *Genes (Basel)*, **11**, 682.
47. Choi, E.H., Suh, S., Sander, C.L., Hernandez, C.J.O., Bulman, E.R., Khadka, N., Dong, Z., Shi, W., Palczewski, K. and Kiser, P.D. (2018) Insights into the pathogenesis of dominant retinitis pigmentosa associated with a D477G mutation in RPE65. *Hum. Mol. Genet.*, **27**, 2225–2243.
48. Waterhouse, A., Bertoni, M., Bienert, S., Studer, G., Tauriello, G., Gumienny, R., Heer, F.T., de Beer, T.A.P., Rempfer, C., Bordoli, L. et al. (2018) SWISS-MODEL: homology modelling of protein structures and complexes. *Nucleic Acids Res.*, **46**, W296–W303.
49. Madeira, F., Park, Y.M., Lee, J., Buso, N., Gur, T., Madhusoodanan, N., Basutkar, P., Tivey, A.R., Potter, S.C. and Finn, R.D. (2019) The EMBL-EBI search and sequence analysis tools APIs in 2019. *Nucleic Acids Res.*, **47**, W636–W641.
50. Robert, X. and Gouet, P. (2014) Deciphering key features in protein structures with the new ENDscript server. *Nucleic Acids Res.*, **42**, W320–W324.
51. Omasits, U., Ahrens, C.H., Muller, S. and Wollscheid, B. (2014) Protter: interactive protein feature visualization and integration with experimental proteomic data. *Bioinformatics*, **30**, 884–886.